AN ELECTROSTATICALLY-ACTUATED MEMS SWITCH FOR POWER APPLICATIONS

Jo-Ey Wong, Jeffrey H. Lang, Martin A. Schmidt
Massachusetts Institute of Technology
Cambridge, MA 02139

ABSTRACT

This paper presents the design, analysis, fabrication, and testing of an electrostatically-actuated MEMS power switch. The device can be switched electrostatically (20 V), pneumatically (1200 Pa), or through combined actuation. Prototype switches carry currents in excess of 400 mA in either current direction with a contact resistance as low as 14 mΩ. Their off-state resistance is higher than the 30 MΩ limit of the test equipment. Breakdown voltages of 300 V have been achieved across their small air gaps. Their nominal switching time is 20 ms. Extended life-time testing has not been carried out but our tests to date show that the prototype switches operate more than 4000 cycles without significant degradation in their contact resistance. Finally, a protective switching scheme is proposed to minimize contact wear due to arcing during switch opening and closing.

INTRODUCTION

Solid-state transistors and conventional electro-magnetic relays have been commonly used in various industrial applications as switching devices to make or break circuits. The former is known for its small size, mass producibility, and easy on-chip integration while the latter for its high stand-off voltage, low on-state resistance, and high current capability. The choice of one type of switching device over the other depends on application requirements. The emergence of MEMS technologies has brought global attention to the possibility of merging conventional macroscopic relay attributes with MEMS device attributes into a new family of switching devices: MEMS based relays/switches. Most MEMS relay/switch studies found in the literature either focus on signal switching applications, such as automatic test equipment [1-5], telecommunications [6-13], and logic operation [14], or are oriented toward technology demonstration [15-21]. Few [22] have addressed the need for a MEMS-based relay/switch tailored for power applications, and that is the goal of this paper.

One of the promising high power applications of MEMS switches is automotive relay replacement. Fifteen million automobiles are manufactured per year in the U.S. and an average car uses approximately 15 relays which is increasing rapidly to as many as 50 per car. This puts the automotive relay market at 225 million relays per year in the U.S. alone. Thus, one important target application for a MEMS switch would be in the replacement of the conventional relay block in an automobile. The intent is to embed MEMS switches at the point of use instead of running wire harnesses across the engine compartment to a relay block. Embedding relays at point of use reduces car weight and power line loss, and improves fuel economy and automobile performance.

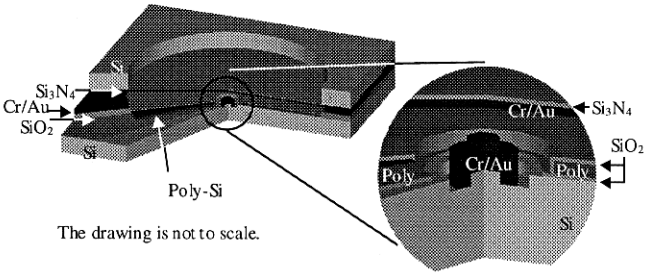

Figure 1: Perspective cross-sectional drawing of device and close-up of contact region.

The key attributes of a power switch are high current-carrying capability and low on-state resistance enabling high power transmission with low loss. Compared to signal switches, switching speed, on-state insertion loss, off-state parasitic capacitive coupling, signal cross-talking noises, and so on are not major issues for power switches. As with signal switches, power switches call for high off-state resistance and high stand-off voltage.

DESIGN AND THEORY

Various actuation mechanisms have been proposed for different micro actuator applications. In the case of the

MEMS relay/switch, the characteristics of primary interest are the attainable force and displacement, power consumption, and ease of fabrication. Piezoelectric mechanisms cannot provide enough displacement without using an actuator of relatively large size due to limitations of real material properties. For thermal actuation mechanisms, there is a trade-off between the thermal response time and the power consumption. The major issues with magnetostatic mechanisms are power consumption, material permeability and IC processing compatibility. The inherent complication with pneumatic actuation lies in its integration with other electronic components and additional pneumatic connections. In the case of electrostatic actuation, the requirement of a large area with a close gap separation for the purpose of generating force of significant magnitude imposes fabrication difficulties.

Our choice of actuation mechanism for the MEMS switch is electrostatics, with pneumatic actuation as a secondary means. Gas pressure actuation requires special packaging to assure air-tight sealing and is used only as a supplemental characterization tool. With minor design modification, our switch is also applicable in pressure control applications, such as pressure switches with tunable threshold pressures controlled by a voltage bias.

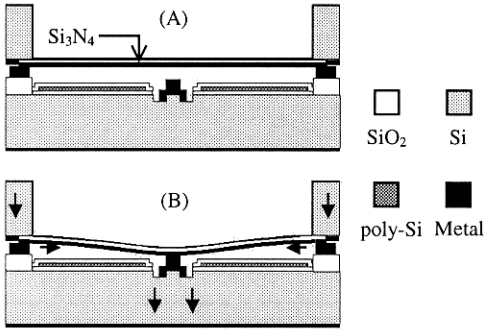

Figure 2: Device cross-section when OFF (A), and when ON (B) with current flow directions.

Our design of a MEMS power switch employs a two-wafer stack structure with a circular LPCVD silicon nitride diaphragm as the moving structure. This hockey-puck power paradigm also possesses favorable features such as good heat dissipation and easy packaging.

The structure of a normally-open MEMS switch is depicted in Figure 1 and Figure 2. With control effort less than the threshold value, no contact is made between the top metallized diaphragm and the bottom contact pedestals, and the MEMS switch is in OFF state (Figure 2A). When the applied pressure or voltage exceeds P_{close} or $V_{pull\text{-}in}$, respectively, current flows vertically through the wafers and radially within the diaphragm (Figure 2B).

Only the single-pole-single-throw (SPST) MEMS switch is considered here. More complicated switches can be constructed by integrating multiple SPST switches. The packaging of an array of electrically parallel MEMS switch cells with different electrical configurations can provide this complexity extension and/or higher current capacity. This approach appears to be more cost effective and more flexible than extending the size of the SPST MEMS switch itself.

The physical effort necessary to actuate the MEMS switch is determined by the distance across the contact gap, the actuation gap separation in the case of electrostatic actuation, and the mechanical properties of the moving diaphragm. The contact gap distance is the deflection that the top diaphragm must deform to make physical contact with the bottom pedestal and its design dimension is prescribed by the thickness of the field oxide. The actuation gap distance is the space across which actuation electric field is applied. The residual in-plane stress, dimension, boundary conditions, and rigidity of the metal-nitride-metal composite diaphragm dictate the diaphragm stiffness.

The relation between applied pressure (p) and the central deflection of a circular diaphragm (δ) with internal stress (σ_0) can be formulated with analytical film-deflection theory [23]. The result is

$$p = \frac{Et}{1-\nu}\left(\frac{7-\nu}{3a^4}\right)\delta^3 + \frac{4Et^3}{3a^4(1-\nu)}\delta + \frac{4\sigma_0 t}{a^2}\delta \qquad (1)$$

where E is the Young's modulus, ν is the Poisson ratio, t is the thickness, and a is the radius of the diaphragm. The first term on the right-hand side of Equation (1) is due to the stretching effect, the second term is due to the bending effect, and third term is due to the residual-stress effect. Stretching becomes the dominant term for very large deflections resulting in a nonlinear p-δ relation and the bending term has higher-order dependency on film thickness.

Our design geometries and choice of materials for the MEMS switch are such that the diaphragm can be modeled as a highly-tensile-stressed thin film, and calculations confirm that the bending and stretching terms combined are less than 0.15% of the stress term. In the highly stressed thin-film limiting case, Equation (1) degenerates to

$$p = \frac{4\sigma_0 t}{a^2}\delta. \qquad (2)$$

Since the design contact gap separation is larger than two thirds of the design actuation gap, the MEMS switch would be electrostatically turned ON under an instability condition. A closed-form expression for the pull-in voltage ($V_{pull\text{-}in}$) in the case of a clamped circular diaphragm [24] is

$$V_{pull-in} = \sqrt{\frac{\gamma_1 \sigma_0 E t g_0^{\,3}}{(1-\nu^2)\varepsilon_0 a^2 f(\gamma_2, k, a)}} \qquad (3)$$

where g_0 = actuation gap separation, ε_0 = permittivity of air, γ_1 = 1.55, γ_2 = 1.65, $k = \sqrt{12(1-\nu^2)/Et^2\sigma_0^{\,2}}$, and $f(\gamma_2, k, a) = 1 + 2[1-\cosh(\gamma_2 ka/2)]/(\gamma_2 ka/2)\sinh(\gamma_2 ka/2)$. The same argument as in pneumatic actuation case applies here; the diaphragm mechanics is dominated by stress and thus Equation (3) can be approximated as

$$V_{pull-in} = \sqrt{\frac{\gamma_1 \sigma_0 t g_0^{\,3}}{\varepsilon_0 a^2}}. \qquad (4)$$

To switch off electrostatically, the actuation voltage will need to drop below to a voltage less than $V_{pull\text{-}in}$ due to the hysteretic nature of electrostatic actuation.

FABRICATION PROCESS

The power MEMS switch consists of two silicon wafers stacked together. A circular silicon nitride diaphragm is formed using bulk-micromaching technologies and serves as the moving structure. A schematic representation of the process sequence for the bottom wafer and top wafer is shown in Figure 3 and Figure 5, respectively. A cross-section drawing of a completed device is shown in Figure 2(A).

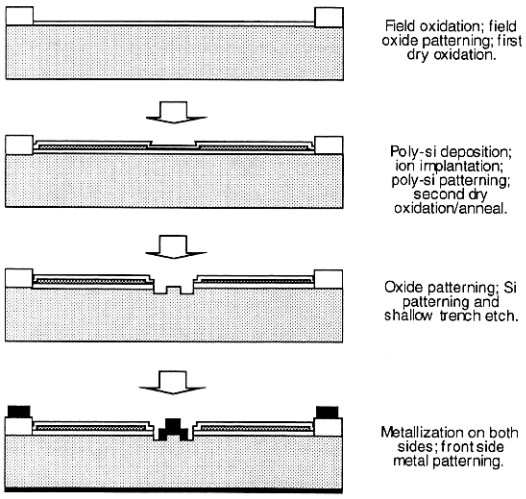

Figure 3: Primary fabrication steps of bottom wafers; the drawings are not to scale.

Bottom wafer processing begins with the growth of a thermal oxide on a low-resistivity silicon wafer. This oxide, whose thickness sets the gap spacing between the contacts when open, is then patterned. Subsequently a dry oxide is grown and a LPCVD poly-silicon layer is deposited. The poly-silicon is then doped using ion implantation and patterned to form the actuation electrode. Following this, a high-temperature anneal in an oxidizing environment is performed and an oxide is grown on the poly-silicon during this anneal. At this stage, the poly-silicon actuation electrode is fully encapsulated within oxides for the purpose of electrical isolation. A photolithography/etch step follows to remove oxides from the contact region as well as to remove oxide from above poly-silicon in the region of contact to this layer. To facilitate four-point-probe measurement for the contact resistance measurement, lead-out from the contact is made with an additional photolithography step followed by a silicon trench-etch. This additional photolithography/trench-etch step also defines the contact pedestal shape (Figure 4). Finally, the contact metal is deposited and patterned on the front side and another layer of metal is deposited on the back.

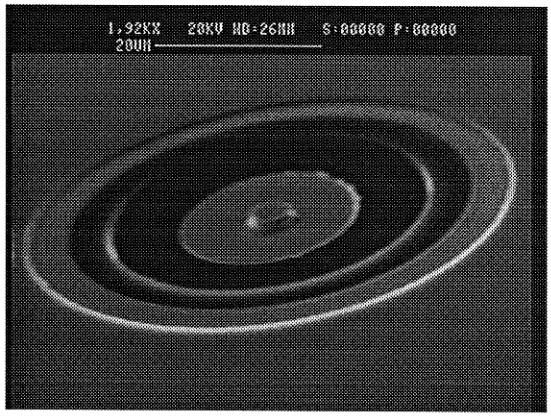

Figure 4: SEM picture of a 3-μm contact pedestal

Top wafer processing begins with the growth of a thin layer of oxide and the deposition of LPCVD silicon nitride on a double-side polished silicon substrate, followed by patterning of the thin films. The tensile-stressed LPCVD silicon nitride will dictate the mechanics of the final moving diaphragm and the thin oxide acts as a future etch stop layer. Next, a photolithography step is performed on the backside of the substrate and a deep RIE etch follows. This through-wafer etch stops at the buried thin oxide layer forming a clamped silicon nitride diaphragm. Metallization on both sides of the substrate completes the top wafer processing.

The top and bottom wafers are then diced, cleaned, aligned and pressed together to bond the facing metals with various bonding approaches as shown in Figure 2(A). Inside metallization is for the contact and bonding purpose while outside metallization is for external connection. The total number of masks used is eight, with three for the top wafers and five for the bottom wafers. The processes are IC-compatible until the final metallization. The contact metal used here is gold because of the low gold-to-gold contact resistance [25, 26] and its ready availability at our facility. Other contact metals may also be exploited to achieve optimal contact performance.

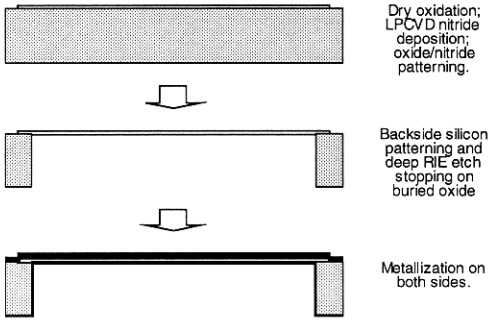

Figure 5: Primary fabrication steps of top wafers; the drawings not to scale.

EXPERIMENTAL RESULTS

To avoid any process uncertainty, the actuation gap separation is measured indirectly through capacitance measurement between the doped poly-silicon and the metallized diaphragm with no actuation. Extra care must be taken to exclude parasitics embedded in the switch. The capacitance of the contact air gap of a typical switch is 14.4 ± 1.4 pF. This capacitance in turn is used to calculate the gap spacing based on a multi-layer parallel-plate capacitance model and yields a gap of 2.79 ± 0.31 μm. Due to the fact that the wafers are mechanically bonded, the discrepancy between the measured gap and the 1 μm design distance is attributed to residues on the bonding surfaces.

For quantitative characterization of the mechanical properties of the diaphragm, pneumatic actuation with special air-tight packaging is used to close the MEMS switch contacts while the contact resistance and the switched current are measured. The contact resistance measurement is made with extra four-point-probe lines leading out to pads from the contacts. The result for the typical switch is shown in Figure 6. The actual off-state resistance of the switches is measured off-line and is higher than the 30 MΩ limit of the ohmmeter. Finally, breakdown voltages of 300 V have been achieved across the small contact gaps.

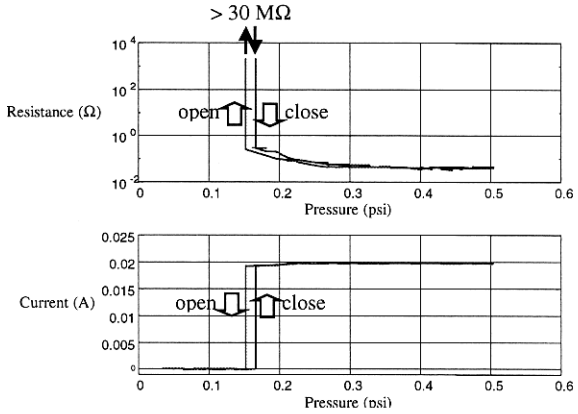

Figure 6: Pneumatic actuation of MEMS switch.

Using the closing pressure of 0.175 psi (1207 Pa) together with the p-δ formulation in Equation (2), the contact air gap separation is found to be 2.74 ± 0.17 μm. This matches well with the actuation gap obtained from capacitance measurement, considering that actuation gap is designed to be only 0.3 μm wider than contact gap.

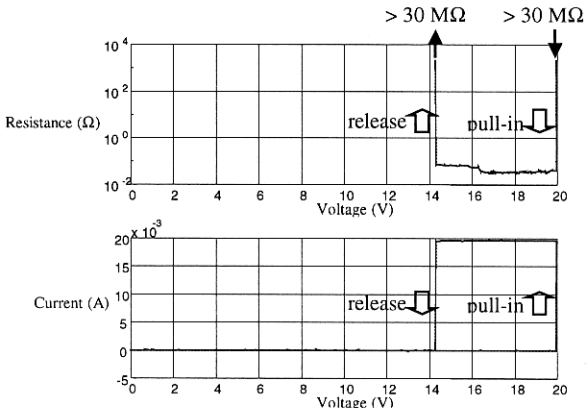

Figure 7: Electrostatic actuation of MEMS switch.

Electrostatic actuation is performed in a similar manner as pneumatic actuation; the contact resistance and switched current are monitored while sweeping the actuation voltage. Given the actuation air gap distance of 2.79 ± 0.31 μm obtained from the capacitance measurement of 14.4 ± 1.4 pF and the geometry and material properties of the switch diaphragm, Equation (4) can be used to predict the pull-in voltage, $V_{pull\text{-}in}$, of 19.92 ± 3.41 V. A typical test result of electrostatic actuation is shown in Figure 7 with $V_{pull\text{-}in}$ = 19.90 V, which agrees with the prediction. Our switches exhibit essentially zero power consumption during steady state because of the nature of electrostatic actuation. It can be seen that the typical

MEMS switch exhibits a 35 mΩ contact resistance while carrying 20 mA of current when actuated either pneumatically (Figure 6) or electrostatically (Figure 7). Our experimental switches can carry currents in excess of 400 mA in either current direction and achieve contact resistances as low as 14 mΩ.

Switching time is acquired by measuring the time delay between the change of the actuation signal V_{act} and that of the responding output signal V_{out} and is found to be on the order of 20ms; see Figure 8. The MEMS switch is not targeted for high-speed application but the development of a faster switch is an ongoing research effort.

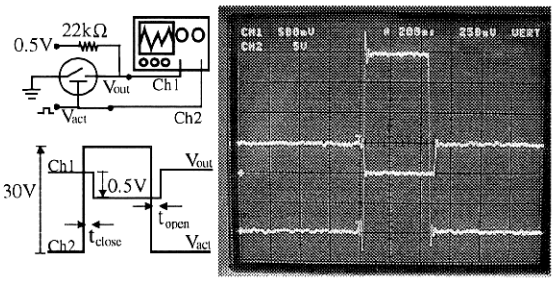

Figure 8: Switching speed measurement ; 0.5V/div for Ch.1, 5V/div for Ch.2, 200ms/div on osscilloscope screen.

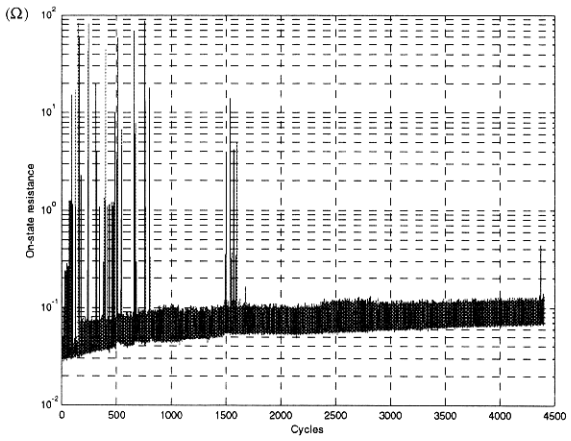

Figure 9: Preliminary life-cycle test results

Figure 9 shows that there is not much contact resistance degradation as it starts from 50 mΩ and settles to 90 mΩ in one run of a preliminary life-cycle test, which is stopped just over 4000 operations. We believe that the lifetime of the mechanically moving device is dictated more by the wear of contacts than by the failure of the diaphragm itself. Since arcing is a well-known cause of contact wear, we propose a switching scheme where the MEMS switch is paralleled with a solid-state transistor and the transistor turns on before and turns off after the MEMS switch; see Figure 10. In this way, the contacts of the MEMS switch are protected from being brought into close vicinity with a high potential difference across them thereby preventing arcing due to hot switching. This scheme enables us to focus on cold-switching in this study of the MEMS power switch behavior, although the device is capable of hot-switching as shown in the switching speed test. This protective circuit can be incorporated with the MEMS switches via on-chip integration or off-chip packaging and will be the subject of future investigation.

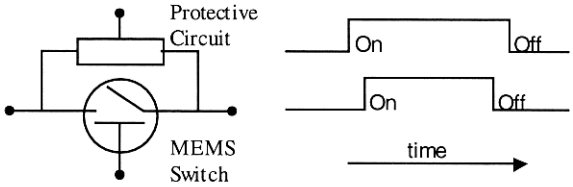

Figure 10: Arcless switching scheme

CONCLUSION

A MEMS switch for power application is proposed, fabricated and tested. One switch cell can carry currents up to 400 mA while exhibiting an on-state resistance as low as 14 mΩ, an off-state resistance in excess of 30 MΩ, and an open-circuit standoff voltage in excess of 300 V. The MEMS switch can be actuated either electrostatically with 20 V or pneumatically with 1200 Pa.

ACKNOWLEDGEMENT

The authors would like to thank the Packard Electric, division of the General Motors Corporation, and the C. P. Clare Corporation for the financial support of this work and the staff of MIT Microsystems Technology Laboratories for technical assistance.

REFERENCES

[1] Drake, J., Jerman, H., Lutze, B., and Stuber, M., "*An Electrostatically Actuated Micro-Relay*", in *Transducers '95, The 8th International Conference on Solid-State Sensors and Actuators, and Eurosensors IX.* 1995. Stockholm, Sweden. p.380-383

[2] Zavracky, P.M., Majumder, S., and McGruer, N.E., "*Micromechanical switches fabricated using nickel surface micromachining*", Microelectromechanical Systems, Journal of, 1997. **6**(1): p. 3-9.

[3] Fullin, E., Gobet, J., Tilmans, H.A.C., and Bergqvist, J., "*A new basic technology for magnetic micro-actuators*", in *Micro Electro Mechanical Systems, 1998.*

MEMS 98. Proceedings., The Eleventh Annual International Workshop on. 1998. p.143-147

[4] Sakata, M., Komura, Y., Seki, T., Kobayashi, K., Sano, K., and Horiike, S., "*Micromachined Relay which Utilizes Single Crystal Silicon Electrostatic Actuator*", in *Micro Electro Mechanical Systems, 1999. MEMS '99. Twelfth IEEE*. 1999. p.21-24

[5] Tilmans, H.A.C., *et al.*, " *A fully-packaged electromagnetic microrelay*", in *Micro Electro Mechanical Systems, 1999. MEMS '99. Twelfth IEEE International Conference on*. 1999. p.25-30

[6] Hannoe, S., Hosaka, H., Kuwano, H., and Yanagisawa, K., "*Mechanical and Electrical Characteristics of Ultra-low-force contacts Used in Micromechanical Relays*", in *Proceedings of the 17th International Conference on Electrical Contacts*. 1994. Nagoya, Japan. p.185-191

[7] Yao, J.J. and Chang, M.F., "*A Surface Micromachined Miniature Switch for Telecommunications Applications with Signal Frequencies from DC up to 4 GHz*", in *Transducers '95, The 8th International Conference on Solid-State Sensors and Actuators, and Eurosensors IX*. 1995. Stockholm, Sweden. p.384-387

[8] Schiele, I., Huber, J., Evers, C., Hillerich, B., and Kozlowski, F., "*Micromechanical relay with electrostatic actuation*", in *Solid State Sensors and Actuators, 1997. TRANSDUCERS '97 Chicago., 1997 International Conference on*. 1997. p.1165 - 1168

[9] Brown, E.R., "*RF-MEMS switches for reconfigurable integrated circuits*", Microwave Theory and Techniques, IEEE Transactions on, 1998. **46**(11): p. 1868-1880.

[10] Goldsmith, C.L., Yao, Z., Eshelman, S., and Denniston, D., "*Performance of Low-Loss RF MEMS Capacitive Switches*", IEEE Microwave and Guided Wave Letters, 1998. **8**(8): p. 269-271.

[11] Nguyen, C.T.-C., Katehi, L.P.B., and Rebeiz, G.M., "*Micromachined devices for wireless communications*", Proceedings of the IEEE, 1998. **86**(8): p. 1756-1768.

[12] Hyman, D., *et al.*, "*GaAs-compatible surface-micromachined RF MEMS switches*", Electronics Letters, 1999. **35**(3): p. 224-226.

[13] Zhou, S., Sun, X.-Q., and Carr, W.N., "*A Monolithic Variable Inductor Network Using Microrelays with Combined Thermal and Electrostatic Actuation*", Journal of Micromechanics and Microengineering, 1999. **9**: p. 45-50.

[14] Hirata, A., Machida, K., Kyuragi, H., and Maeda, M., "*A micromechanical switch as the logic elements for circuits in multi chip mudule on Si (MCM-Si)*", in *Micro Electro Mechanical Systems, 1999. MEMS '99. Twelfth IEEE*. 1999. p.582-587

[15] Petersen, K.E., "*Micromechanical Membrane Switches on Silicon*", I.B.M. Journal of Research and Development, 1979. **23**(4): p. 376-385.

[16] Sakata, M., "*An Electrostatic Microactuator for Electro-Mechanical Relay*", in *Micro Electro Mechanical Systems, 1989, MEMS '89, Proceedings. IEEE*. 1989. p.149-151

[17] Hashimoto, E., Uenishi, Y., and Watabe, A., "*Thermally Controlled Magnetization Microrelay*", in *Solid-State Sensors and Actuators, 1995 and Eurosensors IX.. Transducers '95. The 8th International Conference on*. 1995. p.361-.364

[18] Rogge, B., Schulz, J., Mohr, J., Thommes, A., and Menz, W., "*Fully Batch Fabricated Magnetic Microactuators Using A Two Layer Liga Process*", in *Solid-State Sensors and Actuators, 1995 and Eurosensors IX.. Transducers '95. The 8th International Conference on*. 1995. p.320-323

[19] Roy, S. and Mehregany, M., "*Fabrication of electrostatic nickel microrelays by nickel surface micromachining*", in *Micro Electro Mechanical Systems, 1995, MEMS '95, Proceedings. IEEE*. 1995. p.353-357

[20] Gretillat, M.-A., Yang, Y.-J., Hung, E.S., Rabinovich, V., Ananthasuresh, G.K., De Rooij, N.F., and Senturia, S.D., "*Nonlinear electromechanical behaviour of an electrostatic microrelay*", in *Solid State Sensors and Actuators, 1997. TRANSDUCERS '97 Chicago., 1997 International Conference on*. 1997. p.1141 - 1144

[21] Simon, J., Saffer, S., Sherman, F., and Kim, C.-J., "*Lateral polysilicon microrelays with a mercury microdrop contact*", Industrial Electronics, IEEE Transactions on, 1998. **45**(6): p. 854-860.

[22] Taylor, W.P., Brand, O., and Allen, M.G., "*Fully integrated magnetically actuated micromachined relays*", Microelectromechanical Systems, Journal of, 1998. **7**(2): p. 181-191.

[23] Lin, P., "*The In-situ Measurement of Mechanical Properties of Multi-layer Coatings*", 1990, Massachusetts Institute of Technology: Cambridge, MA.

[24] Osterberg, P.M. and Senturia, S.D., "*M-TEST: A Test Chip for MEMS Material Property Measurement Using Electrostatically Actuated Test Structures*", Journal of Microelectromechanical Systems, 1997. **6**(2): p. 107-118.

[25] Hyman, D. and Mehregany, M., "*Contact physics of gold microcontacts for MEMS*", in *Electrical Contacts, 1998. Proceedings of the Forty-Fourth IEEE Holm Conference on*. 1998. p.133-140

[26] Schimkat, J., "*Contact materials for Microrelays*", in *Micro Electro Mechanical Systems, 1998. MEMS 98. Proceedings., The Eleventh Annual International Workshop on*. 1998. p.190-194